Diverse reactivity model for traffic flow dynamics in Eulerian scope

Md Anowar Hossain (anowar.math.buet@gmail.com)
Kyushu University - Chikushi Campus: Kyushu Daigaku - Chikushi Campus
TANIMOTO Jun
Kyushu University: Kyushu Daigaku

Research Article

Keywords:

Posted Date: May 13th, 2022

DOI: https://doi.org/10.21203/rs.3.rs-1425506/v1

Diverse reactivity model for traffic flow dynamics in Eulerian scope

Md. Anowar Hossain[a)], Jun Tanimoto[a), b)]

[a)] *Interdisciplinary Graduate School of Engineering Sciences, Kyushu University, Kasuga-koen, Kasuga-shi, Fukuoka, 816-8580, Japan.*

[b)] *Faculty of Engineering Sciences, Kyushu University, Kasuga-koen, Kasuga-shi, Fukuoka, 816-8580, Japan.*

Abstract

In this study, a new continuum traffic model is established in consideration of the diverse reactivity effect that emerges from driving attention and the vehicle's inertia. To instigate this diverse reactivity effect, two new functions are introduced, namely, a driver's sensitivity function relying on the flow field's instantaneous density that follows a reverse tendency of optimal velocity function and an inertial equilibrium velocity function assuming the vehicle's inertia coefficient. Comparative analysis is performed using the proposed model and the conventional full velocity difference model. To ascertain the flow field neutralization capability of this model, a neutral stability analysis and the attendant neutral stability condition are derived. The complex behavior of the model near the critical point is investigated via nonlinear analysis, and the wavy solution of the Korteweg-de Vries–Burgers equation is obtained. To verify the analytical solution, a numerical simulation is performed, with the results demonstrating excellent agreement with the obtained theoretical results.

Corresponding author: anowar.math.buet@gmail.com

PACS numbers: 89.40.-a (Transportation); 87.15. Aa (Theory and modeling; Computer simulation)

I. Introduction

The complex behaviors of traffic flow dynamics emerge from the driver's activity, the vehicle's capability, the cooperative or defective neighbor attitude, and the flow field circumstances, all of which have drawn the attention of scientists concerned with the dynamical behavior of complex physics. The multiplex phenomena of the traffic flow field have been investigated following two main approaches: (i) the Eulerian approach, revealing the whole scenario of the traffic flow field based on the laminar fluid flow, and (ii) the Lagrangian approach, focusing on each individual vehicle and including an offshoot widely used for simulation-based research that is termed the cellular automata (CA) traffic model. Meanwhile, to investigate the dynamical behavior of the traffic flow field, various types of traffic flow models have been proposed, including continuum models, [1–6] microscopic models, [7–12] lattice hydrodynamic models, [13–17] and various CA models [18–23] while considering various effects, such as the system time delay effect, the horn effect, the heterogeneous vehicle's effect, and the CA–human-driven mixed-flow effect. However, although an array of traffic models have already been devised, traffic flow analysis is a fundamental aspect of studying the complex behavior of nonlinear sciences, and the majority of previous studies are largely conventional and straightforward, except for several admirable works. [24–31] With this in mind, the focus of the present study is on how driving concentration, or the driver's sensitivity, is affected by the density of the instantaneous flow field under various inertial opposing forces of acceleration and deceleration with vehicles moving along the same roads.

In the early stages of traffic flow analysis, the traffic flow field was treated as a hydrodynamical fluid flow field to investigate the field's complex behavior, with scientists using the only available methodology, the so-called macroscopic approach, to study the field. In 1955, Lighthill, Whitham, and Richards suggested a continuum traffic model, the Lighthill–Whitham–Richards (LWR) model, [1,2] following the first–order continuity equation. The dynamical equation of the macroscopic LWR traffic model is as follows:

$$\frac{\partial \rho}{\partial t} + \frac{\partial (\rho v)}{\partial x} = 0, \tag{1}$$

where x, t, v, and ρ are the space, time, velocity, and density of the traffic flow field, respectively.

However, the velocity–density correlations of the LWR model, which follow the equilibrium state, appeared impractical and, to address this limitation, Payne [3] suggested another macroscopic traffic model considering a relaxation term, with the governing equation of the traffic model as follows:

$$\frac{\partial v}{\partial t} + v\frac{\partial v}{\partial x} = -\frac{\mu}{\rho T}\frac{\partial \rho}{\partial x} + \frac{v_e - v}{T}, \tag{2}$$

where μ and T are the anticipation coefficient and relaxation time, respectively.

Moreover, in 1995, an unrevealed area of the traffic flow field was demonstrated by Bando et al., [7] who established a new traffic model named the optimal velocity (OV) model from the Lagrangian or microscopic standpoint where vehicles are investigated individually. The mathematical formulation of the OV model is as follows:

$$\frac{dv_n(t)}{dt} = a[V[\Delta x_n(t)] - v_n(t)], \quad (3)$$

where a is the sensitivity parameter of all drivers; $V(\Delta x_n(t))$ and $v_n(t)$ are the OV and current velocity of the nth vehicle at time t, respectively; and $\Delta x_n(t)$ is the headway distance between the nth and $n+1$th vehicles at time t, which is measured using $\Delta x_n(t) = x_{n+1}(t) - x_n(t)$.

Meanwhile, in 1998, Helbing and Tilch [10] modified the OV model, in which unrealistic high accelerations and deceleration had been identified, by introducing a negative velocity difference term, with the improved model termed the generalized force model. Although this negative velocity difference adequately enhanced the flow field stability, as Jiang et al. confirmed, the positive velocity difference is supercharged for stabilizing the flow field compared with the negative velocity difference. Following this, in 2001, the full velocity difference (FVD) model [8] was established, the mathematical expression of which is as follows:

$$\frac{dv_n(t)}{dt} = a[V[\Delta x_n(t)] - v_n(t)] + \lambda \Delta v_n(t), \quad (4)$$

where $\Delta v_n(t)$ is the velocity difference between the nth car and the n+1th car at time t, which is quantified by $\Delta v_n(t) = v_{n+1}(t) - v_n(t)$, and λ is another sensitivity coefficient different from a.

Nevertheless, although the traffic flow field is affected by multiple factors, the driver's attitudes and the vehicle's capabilities are the fundamental elements that have a significant effect on the flow field. The driver's attitudes, including "crazy" driving behavior, such as overtaking and slow driving, are the main reasons for traffic jams, whereas there are no road classifications for individual vehicles, especially in densely populated countries such as Bangladesh, India, and Indonesia. For the sake of linearity, the conventional models and their advocates do not consider the effect of the driver's attitude or, more precisely, how driving attention is affected by the instantaneous conditions of the flow field and the vehicle's capabilities when several inertial vehicles share the same road. The present study was thus initiated to explore the unrevealed aspects of the complex behaviors of the traffic flow field. To this end, a continuum traffic flow model is developed in this study considering diverse reactivity effects that emerge because of varying driving attentiveness with the instantaneous density of the flow field when heterogeneous inertial vehicles share the same road. These diverse reactivity effects are introduced by considering two new functions: the driver's sensitivity function and the inertial equilibrium velocity function relying on the density of the flow field and the internal inertia of the vehicle.

The remainder of the paper is organized as follows. Section II explains the formulation of the proposed model before the linear stability of the model is demonstrated in section III. The nonlinear analysis and numerical simulation are then outlined in sections IV and V, respectively. Finally, section VI concludes the work with the main findings.

II. Diverse Reactivity Traffic Model Formulation

In this section, the new traffic model for the diverse reactivity (DR) effect is described in terms of (i) driving attention changes with the current density of the flow field and (ii) various inertial vehicles sharing the same road. The investigation was initially based on the conventional FVD model, with the model formulations initially presented in a microscopic form to facilitate the understanding before being transformed into a continuum system for further investigations. The dynamical equation of the DR model in microscopic form is as follows:

$$\frac{dv_n(t)}{dt} = a(\Delta x_n(t)) \cdot [V_k[\Delta x_n(t)] - v_n(t)] + \lambda \Delta v_n(t), \quad (5)$$

where $a(\Delta x_n(t))$ is the nth driver sensitivity at time t and $V_k[\Delta x_n(t)]$ is the OV of the nth vehicle at time t with k inertial effect.

The model was then converted from the microscopic to the macroscopic system using the following transformations:

$$\begin{aligned} a(\Delta x_n(t)) &\to a(\rho(t)), \\ v_n(t) &\to v(x,t), \\ v_{n+1}(t) &\to v(x+\Delta, t), \\ \mathrm{V}_k[\Delta x_n(t)] &\to \mathrm{V}_k(\rho), \\ \mathrm{V}_k'[\Delta x_n(t)] \to \overline{\mathrm{V}}_k'(h) &\to -\rho^2 \mathrm{V}_k'(\rho), \end{aligned} \quad (6)$$

where $v(x,t)$ and $\rho(x,t)$ denote the velocity and density, respectively, in the continuum system; $h = \frac{1}{\rho}$ represents the headway gaps; and Δ is the adjacent distance between two cars.

Next, the two new functions were introduced, the driver's sensitivity and inertial equilibrium velocity, [32] with the formulations of these functions as follows:

$$a(\rho) = a_{max} - \frac{a_{max} - a_{min}}{1 + \exp[20(5\rho - \rho_m)]}, \quad (7)$$

$$\mathrm{V}_k(\rho) = v_f \cdot \left[\left(1 + \exp\frac{I_k \cdot (\rho/\rho_m - 0.25)}{0.06}\right)^{-1} - 3.72 \times 10^{-6}\right], \quad (8)$$

where a_{max} and a_{min} in Eq. (7) are the upper and lower limit of the driver's sensitivity, respectively; I_k and v_f in Eq. (8) are the inertia coefficient of the nth vehicle and the free flow speed of the flow field, respectively; and ρ_m and ρ are the maximum and instantaneous density, respectively, of the flow field.

In this formulation, the inertia coefficient range is $I_k = (0, 2)$, with the following phenomena observed:

$$I_k = \begin{cases} (0,1);\ \text{for high} - \text{inertial vehicles} \\ 1;\ \text{for medium inertial vehicles} \\ (1,2);\ \text{For low} - \text{inertial vehicles} \end{cases} \quad (9)$$

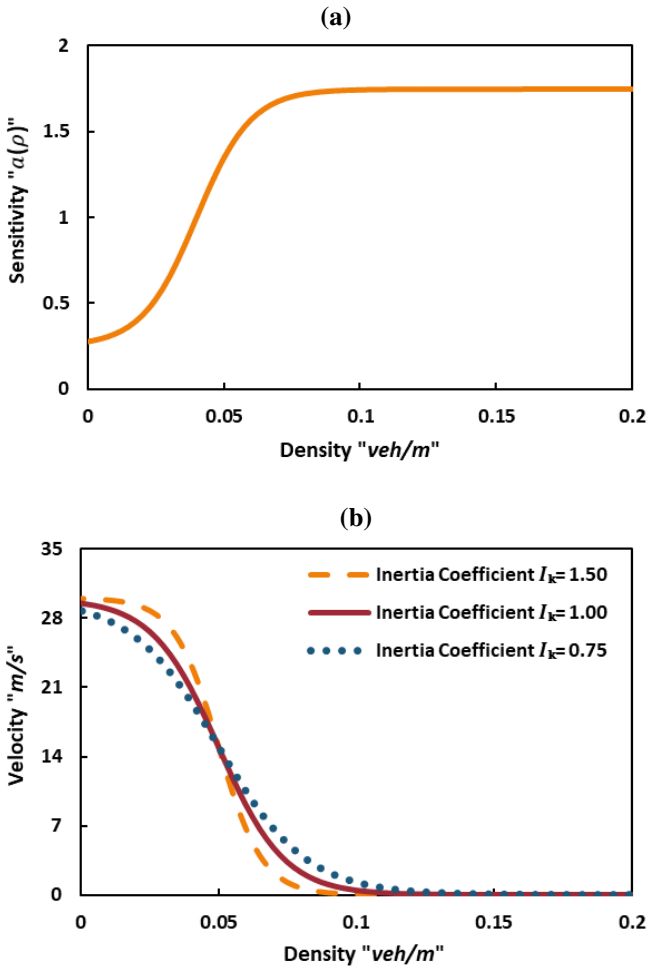

Fig. 1 (a) Line curve describing the history of the driver's sensitivity corresponding to the flow field density and (b) inertial equilibrium velocity profiles.

Using Taylor's series expansion, the term $v(x+\Delta,t)$ can be written in the following form:

$$v(x+\Delta,t) = v(x,t) + v_x\Delta + \frac{1}{2}v_x\Delta^2. \quad (10)$$

The following expression was obtained by substituting Eq. (6) into Eq. (5):

$$\frac{\partial v}{\partial t} + (v - \lambda\Delta)\frac{\partial v}{\partial x} = a(\rho)\cdot[\sum_{k=1}^{m} w_k V_k(\rho) - v] + \frac{\lambda\Delta^2}{2}v_{xx}. \quad (11)$$

Finally, by combining Eq. (11) and Eq. (1), the final form of the DR model was obtained in macroscopic form as follows:

$$\frac{\partial \rho}{\partial t} + \rho\frac{\partial v}{\partial x} + v\frac{\partial \rho}{\partial x} = 0, \quad (12)$$

$$\frac{\partial v}{\partial t} + (v - \lambda\Delta)\frac{\partial v}{\partial x} = a(\rho)\cdot[\sum_{k=1}^{m} w_k V_k(\rho) - v] + \frac{\lambda\Delta^2}{2}v_{xx}.$$

This presents the mathematical expression of the DR model in a continuum system.

Fig. 1a shows the history of the driver's sensitivity and the change in driving concentration behavior in relation to the flow field, whereas **Fig. 1b** shows the inertial equilibrium velocity profiles, introduced considering the vehicle's internal inertia effect. However, a generalized function for several inertial vehicles was also introduced, whereas for simplicity, three types of inertial vehicles were assumed for further investigation: $0 < I_k < 1$ for high-inertial vehicles, $I_k = 1$ for medium inertial vehicles, and $1 < I_k < 2$ for low-inertial vehicles, as shown in **Fig. 1b**.

III. Linear Analysis

Neutral stability analysis was conducted to assess the DR model, specifically in terms of investigating the flow field neutralization capability of the proposed DR model. The DR model can be described in vector form, as follows:

$$\boldsymbol{Ht} + \boldsymbol{AHx} = \boldsymbol{E}, \quad (13)$$

where

$$\boldsymbol{H} = \begin{bmatrix}\rho \\ v\end{bmatrix}, \boldsymbol{A} = \begin{bmatrix} v & \rho \\ 0 & v - \lambda\Delta \end{bmatrix},$$
$$\boldsymbol{E} = \begin{bmatrix} 0 \\ a(\rho)\cdot[\sum_{k=1}^{m} w_k V_k(\rho) - v] + \frac{\lambda\Delta^2}{2}v_{xx} \end{bmatrix}. \quad (14)$$

The eigenvalues of $\boldsymbol{A}$ are given by the following:

$$\lambda_1 = v \text{ and } \lambda_2 = v - \lambda\Delta. \quad (15)$$

It was assumed that v_0, ρ_0, and a_0 are the velocity, density, and driver's sensitivity at the initial state of a homogeneous flow field, respectively:

$$\begin{aligned} \rho(x,t) &= \rho_0, \\ v(x,t) &= v_0, \\ a(x,t) &= a_0, \end{aligned} \quad (16)$$

Subsequently, the following expression was obtained by applying a small disturbance on the uniform flow field:

$$\begin{pmatrix}\rho(x,t) \\ v(x,t) \\ a(x,t)\end{pmatrix} = \begin{pmatrix}\rho_0 \\ v_0 \\ a_0\end{pmatrix} + \begin{pmatrix}\hat{\rho}_k \\ \hat{v}_k \\ \hat{a}_k\end{pmatrix}\exp(ikx + \sigma_k t), \quad (17)$$

where σ_k is the frequency of the waves and k is the number of the wave.

By simplifying Eq. (17) and Eq. (12), the following expression was obtained:

$$(\sigma_k + v_0 ik)\hat{\rho}_k + \rho_0 ik\hat{v}_k = 0, \quad (18)$$

$$a(\rho_0)[\sum_{k=1}^{m} w_k V_k'(\rho_o)]\hat{\rho}_k - \left[a(\rho_0) - \frac{\lambda\Delta^2(ik)^2}{2} + \sigma_k + (v_0 - \lambda\Delta)ik\right]\hat{v}_k = 0.$$

The following quadratic equation could then be obtained from Eq. (18):

$$(\sigma_k + v_0 ik)^2 + (\sigma_k + v_0 ik)\cdot\left[a(\rho_0) + \frac{\lambda\Delta^2 k^2}{2} - \lambda\Delta ik\right] + [a(\rho_0)\ \sum_{k=1}^{m} w_k V_k'(\rho_o)]\cdot(\rho_0 ik) = 0. \quad (19)$$

Consider that $\sigma_k = \sigma_1(ik) + \sigma_2(ik)^2 + \cdots$ .or the stable flow, both roots of σ_k must contain a negative real term. However, the following inequality would be satisfied for the stable traffic flow states:

$$a_{max} - a_{min} + \left[1 + e^{20(5\rho - \rho_m)}\right]\cdot\left[a_{max} + \left(\lambda\Delta + \rho\sum_{k=1}^{m} w_k \cdot V_k'(\rho_0)\right)\right] > 0. \quad (20)$$

Thus, the following neutral stability condition for the DR model was obtained:

$$a_{max} - a_{min} = -\left[1 + e^{20(5\rho - \rho_m)}\right]\cdot\left[a_{max} + \left(\lambda\Delta + \rho\sum_{k=1}^{m} w_k \cdot V_k'(\rho_0)\right)\right], \quad (21)$$

where the imaginary term of σ_k can be described as follows:

$$\mathrm{Im}(\sigma_k) = -k\left(v_0 + \rho\sum_{k=1}^{m} w_k V_k'(\rho_o)\right) + o(k^3). \quad (22)$$

The disturbance progresses from the critical velocity as follows:

$$c(\rho_0) = v_0 + \rho\sum_{k=1}^{m} w_k V_k'(\rho_o). \quad (23)$$

The neutral stability condition described in Eq. (21) illustrates several states of the flow field by following the following inequalities:

i) For the stable state:

$$a_{max} - a_{min} > -\left[1 + e^{20(5\rho - \rho_m)}\right]\cdot\left[a_{max} + \left(\lambda\Delta + \rho\sum_{k=1}^{m} w_k \cdot V_k'(\rho_0)\right)\right]. \quad (24)$$

ii) For the marginal state:

$$a_{max} - a_{min} = -\left[1 + e^{20(5\rho - \rho_m)}\right]\cdot\left[a_{max} + \left(\lambda\Delta + \rho\sum_{k=1}^{m} w_k \cdot V_k'(\rho_0)\right)\right]. \quad (25)$$

iii) For the unstable state:

$$a_{max} - a_{min} < -\left[1 + e^{20(5\rho - \rho_m)}\right]\cdot\left[a_{max} + \left(\lambda\Delta + \rho\sum_{k=1}^{m} w_k \cdot V_k'(\rho_0)\right)\right]. \quad (26)$$

This presents the neutral stability criteria of the proposed DR model.

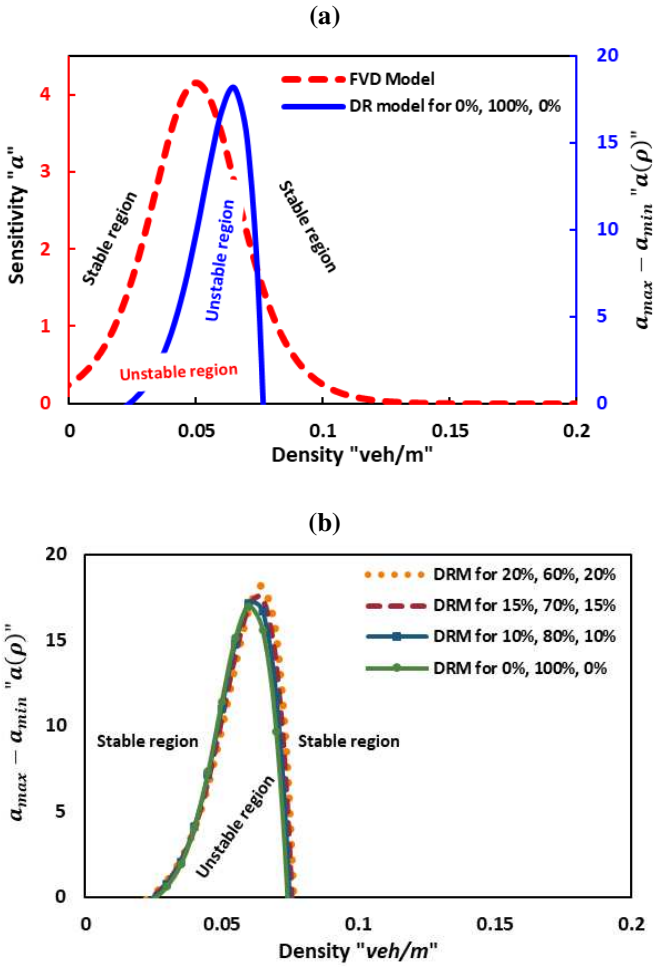

Fig. 2. Phase diagram for the sensitivity–headway space. (a) The solid blue line indicates the neutral stability for the DR mode, whereas the dashed red line denotes the same for the FVD model, and (b) the line curves demonstrated the neutral stability history for the DR mode in various state.

Fig. 2 shows the flow field neutralization history, as described in Eq. (21), of the conventional FVD model and the proposed DR model under various conditions. Here, the DR model was not in line with the conventional FVD model in terms of identifying the unstable region, suggesting a new unstable region on the flow field, whereas most followers of the conventional model [33–35] shared the same unstable zones, albeit highlighting increases and/or decreases in the instability of the flow field. Furthermore, the DR model suggested a higher unstable region for the intermediate density and identified a highly stable flow for low- and high-density region, where a smaller $a_{max} - a_{min}$ ensures higher stability of the flow field compared with the conventional FVD model, as shown in **Fig. 2a**. The instability of the flow field identified by the DR model steadily increased with the increase in the proportions of low-inertial and high-inertial vehicles, as shown in **Fig. 2b**.

IV. Nonlinear Analysis

A small disturbance that emerges, i.e., stop-and-go wave phenomena, was imposed on the flow field at the initial stage to study the complex behavior of the traffic flow. Here, nonlinear analysis of the DR model was performed in terms of the critical point to observe the flow behavior, with a new coordinate system introduced as follows: [36]

$$z = x - ct. \tag{27}$$

The following equations were obtained by combining Eq. (12) and Eq. (27):

$$\begin{aligned} -c\rho_z + q_z &= 0, \\ -cv_z + (v - \lambda\Delta) &= a(\rho)\cdot[\textstyle\sum_{k=1}^{m} w_k V_k(\rho) - v] + \\ &\quad \tfrac{\lambda\Delta^2}{2} v_{zz}, \end{aligned} \tag{28}$$

where $q = \rho v$ indicates that the traffic flux comes from the product of the density and the velocity. The first and second derivatives of the flow velocity can be written as follows:

$$\begin{aligned} v_z &= \tfrac{c\rho_z}{\rho} - \tfrac{q\rho_z}{\rho^2}, \\ v_{zz} &= \tfrac{c\rho_{zz}}{\rho} - \tfrac{2c\rho_z^2}{\rho^2} - \tfrac{q\rho_{zz}}{\rho^2} + \tfrac{2q\rho_{zz}^2}{\rho^3}. \end{aligned} \tag{29}$$

By substituting Eq. (29) into Eq. (28), the following expression was obtained:

$$\begin{aligned} &-c\left(\tfrac{c\rho_z}{\rho} - \tfrac{q\rho_z}{\rho^2}\right) + \left(\tfrac{q}{\rho} - \lambda\Delta\right)\left(\tfrac{c\rho_z}{\rho} - \tfrac{q\rho_z}{\rho^2}\right) = a(\rho)\cdot \\ &\left[\textstyle\sum_{k=1}^{m} w_k V_k(\rho) - \tfrac{q}{\rho}\right] + \tfrac{\lambda\Delta^2}{2}\left(\tfrac{c\rho_{zz}}{\rho} - \tfrac{2c\rho_z^2}{\rho^2} - \tfrac{q\rho_{zz}}{\rho^2} + \right. \\ &\left.\tfrac{q\rho_z^2}{\rho^3}\right). \end{aligned} \tag{30}$$

The flow flux q can be expressed as follows:

$$q = a(\rho)\cdot[\textstyle\sum_{k=1}^{m} w_k V_k(\rho)] + b_1\rho_z + b_2\rho_{zz}. \tag{31}$$

By substituting Eq. (31) into Eq. (30), the following expression could be obtained:

$$\begin{aligned} &-c\left(\tfrac{c\rho_z}{\rho} - \tfrac{(\rho[\sum_{k=1}^{m} w_k V_k(\rho)] + b_1\rho_z + b_2\rho_{zz})\rho_z}{\rho^2}\right) + \\ &\left(\tfrac{\rho[\sum_{k=1}^{m} w_k V_k(\rho)] + b_1\rho_z + b_2\rho_{zz}}{\rho} - \lambda\Delta\right)\left(\tfrac{c\rho_z}{\rho} - \right. \\ &\left.\tfrac{(\rho[\sum_{k=1}^{m} w_k V_k(\rho)] + b_1\rho_z + b_2\rho_{zz})\rho_z}{\rho^2}\right) = a(\rho)\cdot \\ &\left[\textstyle\sum_{k=1}^{m} w_k V_k(\rho) - \tfrac{\rho[\sum_{k=1}^{m} w_k V_k(\rho)] + b_1\rho_z + b_2\rho_{zz}}{\rho}\right] + \\ &\tfrac{\lambda\Delta^2}{2}\left(\tfrac{c\rho_{zz}}{\rho} - \tfrac{2c\rho_z^2}{\rho^2} - \tfrac{(\rho[\sum_{k=1}^{m} w_k V_k(\rho)] + b_1\rho_z + b_2\rho_{zz})\rho_{zz}}{\rho^2} + \right. \\ &\left.\tfrac{2(\rho[\sum_{k=1}^{m} w_k V_k(\rho)] + b_1\rho_z + b_2\rho_{zz})\rho_z^2}{\rho^3}\right). \end{aligned} \tag{32}$$

The values of b_1 and $b_2$could be obtained by equating the coefficients of ρ_z and ρ_{zz}, respectively, in Eq. (32) as follows:

$$\begin{aligned} b_1 &= \tfrac{c}{a(\rho)}(c + \lambda\Delta) - \tfrac{1}{a(\rho)}(2c + \lambda\Delta)\cdot \\ &\left(\textstyle\sum_{k=1}^{m} w_k V_k(\rho)\right) + \tfrac{1}{a(\rho)}[\textstyle\sum_{k=1}^{m} w_k V_k(\rho)]^2, \end{aligned} \tag{33}$$

$$b_2 = \tfrac{\lambda\Delta^2}{2a(\rho)}\left[c - \left(\textstyle\sum_{k=1}^{m} w_k V_k(\rho)\right)\right].$$

Considering that $\rho = \rho_h + \hat{\rho}(x,t)$ is close to the linear stability criteria, the following equation could be obtained using Taylor's expansions for neglecting the higher-order terms of $\hat{\rho}$:

$$\begin{aligned} \rho\left(\textstyle\sum_{k=1}^{m} w_k V_k(\rho)\right) &\approx \rho_h\left(\textstyle\sum_{k=1}^{m} w_k V_k(\rho)\right) + \\ &\left(\rho\left(\textstyle\sum_{k=1}^{m} w_k V_k(\rho)\right)\right)_\rho \Big|_{\rho=\rho_h} \hat{\rho} + \\ &\tfrac{1}{2}\left(\rho\left(\textstyle\sum_{k=1}^{m} w_k V_k(\rho)\right)\right)_{\rho\rho} \Big|_{\rho=\rho_h} \hat{\rho}^2. \end{aligned} \tag{34}$$

The following expression could be obtained by substituting Eq. (34) into Eq. (28) and then transforming $\hat{\rho}$ into ρ:

$$\begin{aligned} &-c\rho_z + \left[\left(\rho\left(\textstyle\sum_{k=1}^{m} w_k V_k(\rho)\right)\right)_\rho + \right. \\ &\left.\left(\rho\left(\textstyle\sum_{k=1}^{m} w_k V_k(\rho)\right)\right)_{\rho\rho}\rho\right]\rho_z + b_1\rho_{zz} + b_2\rho_{zzz} = 0. \end{aligned} \tag{35}$$

The following transformations were performed using Eq. (35):

$$\begin{aligned} U &= -\left[\left(\rho\left(\textstyle\sum_{k=1}^{m} w_k V_k(\rho)\right)\right)_\rho + \right. \\ &\left.\left(\rho\left(\textstyle\sum_{k=1}^{m} w_k V_k(\rho)\right)\right)_{\rho\rho}\rho\right], \\ X &= mx, \\ T &= -mt. \end{aligned} \tag{36}$$

Then, the following standard Korteweg-de Vries (KdV)–Burgers equation was obtained after performing the transformation:

$$U_T + UU_x - mb_1U_{xx} - m^2b_2U_{xxx} = 0. \tag{37}$$

Finally, the following analytical solution could be obtained from the standard KdV–Burgers equation described in Eq. (37):

$$\begin{aligned} U = &-\tfrac{3(-mb_1)^2}{25(-m^2b_2)}\left[1 + 2\tanh\left(\pm\tfrac{-mb_1}{10m^2}\right)\left(X + \tfrac{6((-mb_1)^2)}{25(-m^2b_2)}T + \varepsilon_0\right)\right. \\ &\left. + \tanh^2\left(\pm\tfrac{-mb_1}{10m^2}\right)\left(X + \tfrac{6((-mb_1)^2)}{25(-m^2b_2)}T + \varepsilon_0\right)\right]. \end{aligned} \tag{38}$$

where ε_0 indicates an arbitrary constant.

V. Numerical Simulations

A numerical simulation was performed to verify the analytical solutions of the proposed DR model. The discretization process followed to obtain an explicit form of the model, with the following equations obtained through discretizing Eq. (12):

$$\rho_i^{j+1} = \rho_i^j + \frac{\Delta t}{\Delta x}\rho_i^j\left(v_i^j - v_{i+1}^j\right) + \frac{\Delta t}{\Delta x}v_i^j\left(\rho_i^j - \rho_{i+1}^j\right) \quad (39)$$

$$\text{(a) If } v_i^j < c_i^j,$$

$$v_i^{j+1} = v_i^j - \frac{\Delta t}{\Delta x}\rho_i^j\left(v_i^j - c_i^j\right)\left(v_{i+1}^j - v_i^j\right) + a(\rho)\cdot \Delta t\left[\sum_{k=1}^{m} w_k V_k\left(\rho_i^j\right) - v_i^j\right] + \frac{\Delta t\, c_i^j\, \Delta}{2(\Delta x)^2}\left(v_{i+1}^j - 2v_i^j + v_{i-1}^j\right). \quad (40)$$

$$\text{(b) If } v_i^j < c_i^j,$$

$$v_i^{j+1} = v_i^j - \frac{\Delta t}{\Delta x}\rho_i^j\left(v_i^j - c_i^j\right)\left(v_i^j - v_{i-1}^j\right) + a(\rho)\cdot \Delta t\left[\sum_{k=1}^{m} w_k V_k\left(\rho_i^j\right) - v_i^j\right] + \frac{\Delta t\, c_i^j\, \Delta}{2(\Delta x)^2}\left(v_{i+1}^j - 2v_i^j + v_{i-1}^j\right), \quad (41)$$

where $c_i^j = \frac{\lambda}{\rho_i^j}$.

At the initial stage, a small disturbance was introduced, assuming the average density ρ_0, in the flow field using the Herrmann–Kerner [32] formula:

$$\rho(x,0) = \rho_0 + \Delta\rho_0\left\{\cosh^{-2}\left[\frac{160}{L}\left(x - \frac{5L}{16}\right)\right] - \frac{1}{4}\cosh^{-2}\left[\frac{40}{L}\left(x - \frac{11L}{32}\right)\right]\right\}, \quad (42)$$

where ρ_0 is the initial flow field density, $\Delta\rho_0$ is the density fluctuations, and L is the length of the road.

A cyclic boundary condition was imposed on the numerical simulation, which took the following form:

$$\rho(L,t) = \rho(0,t) \text{ and } v(L,t) = v(0,t). \quad (43)$$

Meanwhile, the following parameter settings were used in the simulation: $\rho_m = 0.2$ veh/m, $\Delta\rho_0 = 0.01$ veh/m, $\Delta x = 100$ m, $\Delta t = 1$ s, $a_{max} = 1.5$, $a_{min} = 0.5$, $\lambda = 0.5$, $L = 32.2$ km, and $v_f = 30$ m/s, and $I_k = 1.5, 1.0, 0.75$ for the low-, medium-, and high-inertial vehicles, respectively.

Fig. 3 shows the results of the comparative analysis of the traffic flux fundamental diagrams for the conventional FVD model for $a = 1$ and the proposed DR model, with the average sensitivity $\left(\frac{a_{max}+a_{min}}{2}\right) = 1$, whereas the flow field was investigated for 1,000 s. However, various traffic flux tendencies of the DR model were observed throughout the flow field densities, i.e., the free flow state, metastable state, and congested state. In the free flow and metastable states, the conventional FVD model (the solid green line) was superior to the DR model (blue dashed line) when all the vehicles were considered with the same inertia effect for $I_k = 1.0$ (medium inertial vehicles). This was because several internal noises that oppressed the flow efficiency emerged with the DR model for the time-varying driver's sensitivity despite being considered homogeneous vehicles, whereas the conventional FVD model fully relied on the time-constant driver's sensitivity and on homogeneous vehicles, from which none of the internal noise originated on the flow field. By contrast, the DR model outperformed the conventional FVD model in the congested state. This is feasible since the new driver's sensitivity function ensures higher driving attention in the high-density region to avoid collisions by confirming the optimum use of the headway gaps in the congested region; this is a major limitation of the conventional FVD model because of the time-constant driver's sensitivity.

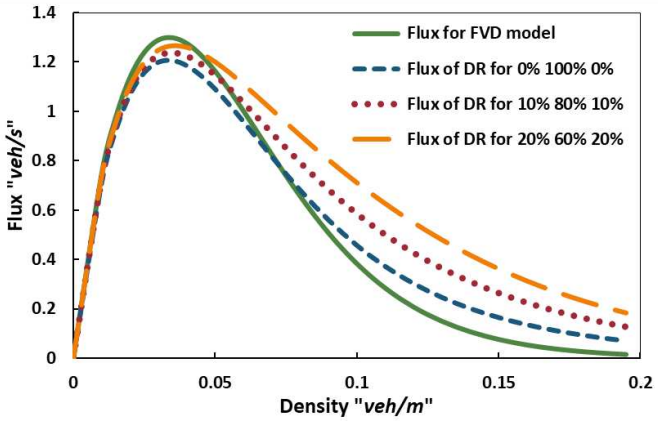

Fig. 3. Fundamental diagram for traffic flux/flow field density of the FVD and DR models under various conditions.

Further investigations were conducted using the DR model to investigate the vehicle's inertia effects on the traffic flow field when several inertial vehicles must share the same road. Although various combinations of inertial vehicle proportions exist, for simplicity, the simulation relied on three types of inertial vehicles: $I_k = 1.5$, 1.0, and 0.75 for the low-, medium-, and high-inertial vehicles, respectively, that are represented by the blue dashed line, the red dotted line, and the orange dashed line, respectively, in **Fig. 3**. This figure demonstrates that the traffic flux significantly improved in the metastable and congested regions with the increase in the proportions of the low- and high-inertial vehicles. Thus, the proposed DR model was found to be more efficient for the metastable and congested regions than the conventional FVD model.

VI. Conclusions

The present study was designed to assess the complex behavior of the traffic flow field in relation to DR effects, evolved for time-varying driving attentiveness when several inertial vehicles share the same road. A continuum traffic model was proposed, termed the DR model, by imposing the following effects: (i) driving concentration that was gradually enhanced with the increase in flow field density following the reverse tendency of the OV function, effect and (ii) the vehicle's internal inertia that depends on the vehicle size and is introduced by an inertial equilibrium velocity function considering the vehicle's inertia coefficient effect. Notably, the DR model was highly efficient in terms of flow field neutralization capability, with the model suggesting a different unstable area compared with the conventional FVD model; this was confirmed via the neutral stability analysis. Nevertheless, it was found that the DR model was inferior in low-density regions, whereas it demonstrated a better performance in congested regions than the conventional FVD model. To gain a better understanding of the complex behavior of the DR model, a nonlinear analysis was performed that provided the KdV–Burgers equation containing a wavy propagation solution for the flow field. Finally, a numerical simulation was conducted to verify the analytical solutions, with excellent agreement between the numerical and analytical results.

Acknowledgments

This study was partially supported by the Grant-in-Aid for Scientific Research (KAKENHI) from JSPS (Grant Nos. JP 19KK0262, JP 20H02314, and JP 20K21062) awarded to Professor Tanimoto.

References

[1] W. G. B. Lighthill M.J., *On Kinematic Waves II. A Theory of Traffic Flow on Long Crowded Roads*, Proc. R. Soc. London. Ser. A. Math. Phys. Sci. **229**, 317 (1955).

[2] P. I. Richards, *Shock Waves on the Highway*, Oper. Res. **4**, 42 (1956).

[3] H. J. Payne, *Mathematical Models of Public Systems*, Simul. Counc. **1**, 51 (1971).

[4] M. A. Hossain and J. Tanimoto, *The "Backward-Looking" Effect in the Continuum Model Considering a New Backward Equilibrium Velocity Function*, Nonlinear Dyn. 2021 1 (2021).

[5] Y. Xue, Y. Zhang, D. Fan, P. Zhang, and H. di He, *An Extended Macroscopic Model for Traffic Flow on Curved Road and Its Numerical Simulation*, Nonlinear Dyn. **95**, 3295 (2019).

[6] N. Davoodi, A. R. Soheili, and S. M. Hashemi, *A Macro-Model for Traffic Flow with Consideration of Driver's Reaction Time and Distance*, Nonlinear Dyn. **83**, 1621 (2016).

[7] M. Bando, K. Hasebe, A. Nakayama, A. Shibata, and Y. Sugiyama, *Dynamical Model of Traffic Congestion and Numerical Simulation*, Phys. Rev. E **51**, 1035 (1995).

[8] R. Jiang, Q. Wu, and Z. Zhu, *Full Velocity Difference Model for a Car-Following Theory*, Phys. Rev. E - Stat. Physics, Plasmas, Fluids, Relat. Interdiscip. Top. **64**, 4 (2001).

[9] M. A. Hossain, K. M. A. Kabir, and J. Tanimoto, *Improved Car-Following Model Considering Modified Backward Optimal Velocity and Velocity Difference with Backward-Looking Effect*, J. Appl. Math. Phys. **9**, 242 (2021).

[10] D. Helbing and B. Tilch, *Generalized Force Model of Traffic Dynamics*, Phys. Rev. E - Stat. Physics, Plasmas, Fluids, Relat. Interdiscip. Top. **58**, 133 (1998).

[11] J. Tanimoto, *Traffic Flow Analysis Dovetailed with Evolutionary Game Theory*, in *Springer 6* (2015), pp. 159–182.

[12] M. A. Hossain and J. Tanimoto, *A Microscopic Traffic Flow Model for Sharing Information from a Vehicle to Vehicle by Considering System Time Delay Effect*, Phys. A Stat. Mech. Its Appl. **585**, 126437 (2022).

[13] T. Nagatani, *Chaotic Jam and Phase Transition in Traffic Flow with Passing*, Phys. Rev. E **60**, 1535 (1999).

[14] H. X. Ge, S. Q. Dai, Y. Xue, and L. Y. Dong, *Stabilization Analysis and Modified Korteweg–de Vries Equation in a Cooperative Driving System*, Phys. Rev. E **71**, 066119 (2005).

[15] T. Nagatani, *Jamming Transition in a Two-Dimensional Traffic Flow Model*, Phys. Rev. E **59**, 4857 (1999).

[16] Y.-R. Kang and D.-H. Sun, *Lattice Hydrodynamic Traffic Flow Model with Explicit Drivers' Physical Delay*, Nonlinear Dyn. 2012 713 **71**, 531 (2012).

[17] T. Wang, Z. Gao, J. Zhang, and X. Zhao, *A New Lattice Hydrodynamic Model for Two-Lane Traffic with the Consideration of Density Difference Effect*, Nonlinear Dyn. 2013 751 **75**, 27 (2013).

[18] J. Matsukidaira and K. Nishinari, *Euler-Lagrange Correspondence of Cellular Automaton for Traffic-Flow Models*, Phys. Rev. Lett. **90**, 088701 (2003).

[19] K. Gao, R. Jiang, S.-X. Hu, B.-H. Wang, and Q.-S. Wu, *Cellular-Automaton Model with Velocity Adaptation in the Framework of Kerner's Three-Phase Traffic Theory*, Phys. Rev. E **76**, 026105 (2007).

[20] B. S. Kerner, S. L. Klenov, and M. Schreckenberg, *Simple Cellular Automaton Model for Traffic*

Breakdown, Highway Capacity, and Synchronized Flow, Phys. Rev. E **84**, 046110 (2011).

[21] Y. Xue, X. Wang, B. Cen, P. Zhang, and H. He, *Study on Fuel Consumption in the Kerner–Klenov–Wolf Three-Phase Cellular Automaton Traffic Flow Model*, Nonlinear Dyn. 2020 1021 **102**, 393 (2020).

[22] Z. Li, Q. Qin, W. Li, S. Xu, Y. Qian, and J. Sun, *Stabilization Analysis and Modified KdV Equation of a Car-Following Model with Consideration of Self-Stabilizing Control in Historical Traffic Data*, Nonlinear Dyn. **91**, 1113 (2018).

[23] Y. Zhang, M. Zhao, D. Sun, and C. Dong, *An Extended Continuum Mixed Traffic Model*, Nonlinear Dyn. **103**, 1891 (2021).

[24] W. G. B. Lighthill M.J., *On Kinematic Waves I. Flood Movement in Long Rivers*, Proc. R. Soc. London. Ser. A. Math. Phys. Sci. **229**, 281 (1955).

[25] P. Berg, A. Mason, and A. Woods, *Continuum Approach to Car-Following Models*, Phys. Rev. E **61**, 1056 (2000).

[26] A. S. De Wijn, D. M. Miedema, B. Nienhuis, and P. Schall, *Criticality in Dynamic Arrest: Correspondence between Glasses and Traffic*, Phys. Rev. Lett. **109**, 228001 (2012).

[27] J. Matsukidaira and K. Nishinari, *Euler-Lagrange Correspondence of Cellular Automaton for Traffic-Flow Models*, Phys. Rev. Lett. **90**, 4 (2003).

[28] N. Mitarai and H. Nakanishi, *Spatiotemporal Structure of Traffic Flow in a System with an Open Boundary*, Phys. Rev. Lett. **85**, 1766 (2000).

[29] H. K. Lee, R. Barlovic, M. Schreckenberg, and D. Kim, *Mechanical Restriction versus Human Overreaction Triggering Congested Traffic States*, Phys. Rev. Lett. **92**, 238702 (2004).

[30] E. Tomer, L. Safonov, and S. Havlin, *Presence of Many Stable Nonhomogeneous States in an Inertial Car-Following Model*, Phys. Rev. Lett. **84**, 382 (2000).

[31] H. Y. Lee, H. W. Lee, and D. Kim, *Origin of Synchronized Traffic Flow on Highways and Its Dynamic Phase Transitions*, Phys. Rev. Lett. **81**, 1130 (1998).

[32] M. Herrmann and B. S. Kerner, *Local Cluster Effect in Different Traffic Flow Models*, Phys. A Stat. Mech. Its Appl. **255**, 163 (1998).

[33] T. Nagatani, *Thermodynamic Theory for the Jamming Transition in Traffic Flow*, Phys. Rev. E - Stat. Physics, Plasmas, Fluids, Relat. Interdiscip. Top. **58**, 4271 (1998).

[34] H. Kuang, Z. P. Xu, X. L. Li, and S. M. Lo, *An Extended Car-Following Model Accounting for the Honk Effect and Numerical Tests*, Nonlinear Dyn. **87**, 149 (2017).

[35] C. Chen, R. Cheng, and H. Ge, *An Extended Car-Following Model Considering Driver's Sensory Memory and the Backward Looking Effect*, Phys. A Stat. Mech. Its Appl. **525**, 278 (2019).

[36] R. Jiang, Q. S. Wu, and Z. J. Zhu, *A New Continuum Model for Traffic Flow and Numerical Tests*, Transp. Res. Part B Methodol. **36**, 405 (2002).